1. Aims and purpose of the satellite

The Atmosphere-Ionosphere coupling Explorer (AICE) is proposed to investigate the coupling effect between the atmosphere and ionosphere by deploying a low-earth orbiting satellite to perform in-situ measurements. The coupling process between ionosphere, magnetosphere and thermosphere aroused scientists' interest from 20th century. These coupling processes have been explored by numerous satellites and ground observations. But several interesting phenomena are found to be associated to the interaction even lower, between the ionosphere and troposphere, or even lithosphere in the past decades. In 1964 Alaska earthquake, ionospheric disturbances before the earthquake are firstly reported [Davies & Baker, 1965; Moore, 1964]. Recently, the electron density slightly below the medium value of quiet time before strong earthquakes are also identified by the GPS-measured TEC and this anomaly last a few days [see Figure 1.1, Le et al., 2013]. Although the mechanism of these coupling processes between ionosphere and lithosphere are still not clear, some theoretical models are proposed to interpret that the ionospheric disturbance is possibly triggered from the lower atmosphere, or even under ground. One of the recent published models is that an electric field produced by stressed rocks will produce ions at earthquake fault zone by field ionization, as Figure 1.2 shown [Kuo, et al., 2011]. Ions propagates to the bottom of ionosphere by the vertical electric field and it generates an electric field disturbance. The disturbed electric field in the ionosphere drives a plasma $\vec{E} \times \vec{B}$ motion and propably produce the plasma bubble. Then the plasma bubble propagates upward along the magnetic field line to the upper ionosphere. This electric field penetration has been observed by INTERCOSMOS-BULGARIA-1300 in 1981 [Gousheva et al, 2009]. The 2-10 mV/m increasing in vertical component was observed in the upper ionosphere (h=800-900km) in 2 month. Their results conclude that the earthquake with magnitude 4.8-7.9 could generate the electric field disturbance in the ionosphere before earthquakes. According to the statistics from U. S. Geological Survey [see Figure1.3, from U. S. Geological Survey website], more than 1,500 earthquakes are recorded in the past year with the magnitude M greater than 5 (about 5 earthquakes per day). Unfortunately INTERCOSMOS-BULGARIA-1300 does not carry any plasma instrument onboard to diagnose the plasma change after the variation of the electric field and its circular orbit kept the satellite fly in the same height to be unable to detect the vertical propagation of the coupling process.

In the other hand, the other turbulence sources of the electric field such as thunderstorm also received attentions in the past decades [Velinov & Tonev, 1995]. There are more than dozens of thunderstorms existing on the earth surface simultaneously. Although lacking of the direct electric field measurement, the theoretical model predicts that the electric field generated by thunderstorms is able to penetrate from cloud top to the ionosphere and forms an electron density irregularities by similar mechanism as the preceding ionospheric disturbance of earthquake [Park & Dejnakarintra, 1973]. The Transient Luminous Events (TLEs), such as

sprite, elve, blue jet, and gigantic jet, are the phenomena of the electrical breakdowns above thunderclouds [Fukunishi et al, 1996; Pasko et al., 1997; Pasko, 2003; Krehbiel et al., 2008]. These TLEs are identified to be related to energetic lightening activity directly [Hu et al., 2002], and it is also expected that the electric field penetration of these TLEs events are more efficient. These TLEs sometime can reach bottom of ionosphere, approximately 85 km height, to contribute an upward current to ionosphere as part of the global electric circuit [Rycroft, 2006] and also play an important roles in the coupling process between ionosphere and atmosphere.
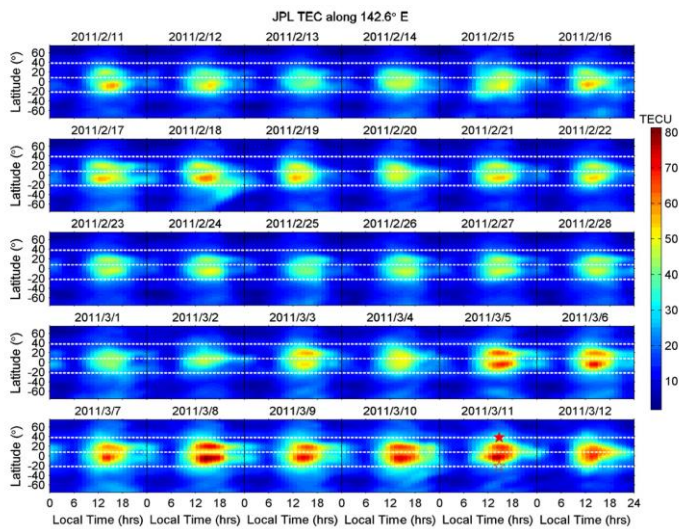

Figure1.1 The TEC disturbance occurred before the the Tohoku-Oki earthquake. The latitude–time-TEC plots extracted from the JPL TEC along 142.37_E from November 2, 2011 to December 3, 2011. The solid and open start symbols are the epicenter and corresponding conjugate point of the Tohoku-Oki earthquake. [Le et al., 2013]
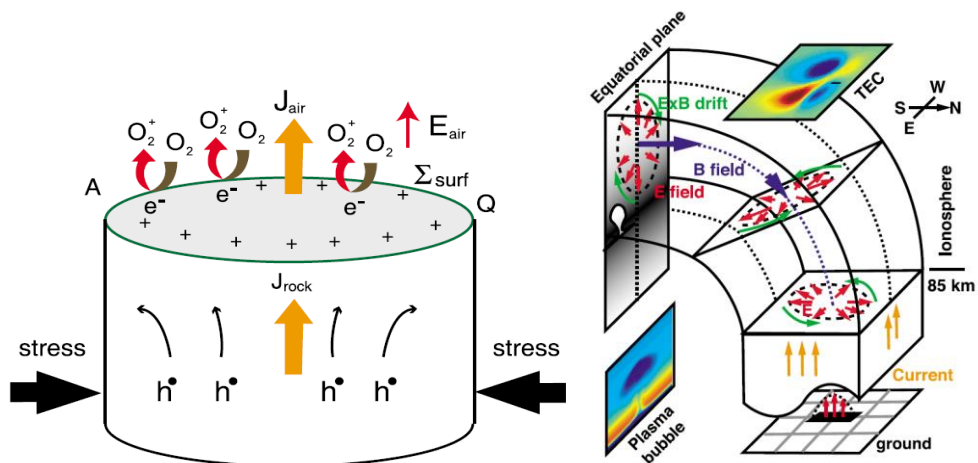

Figure 1.2 Schematic diagram of the electric field formation electric coupling between the ionosphere before the earthquake.
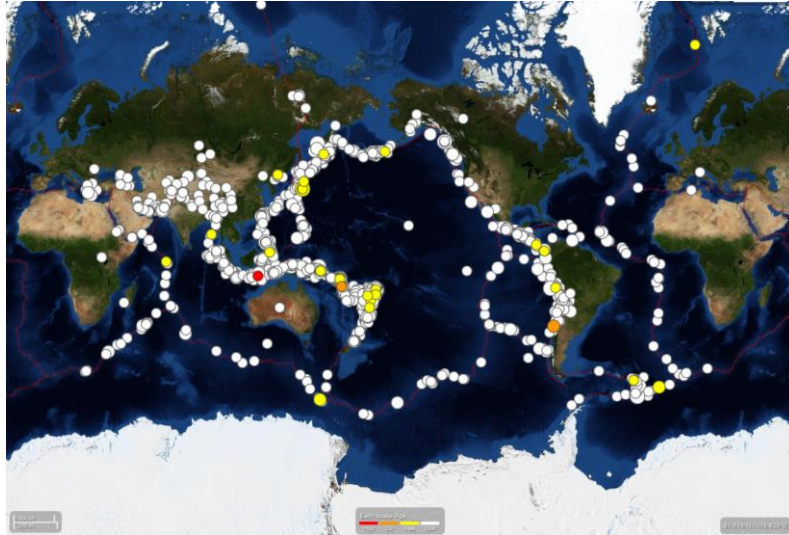
*Figure*1.3 Global occurrence of earthquakes M >5. [U. S. Geological Survey website]

Therefore, the Atmosphere – Ionosphere Coupling Explorer (AICE) mission is proposed here to observe the plasma chracteristics as well as the electric and magnetic fields interaction from 300 to 700 km and investigate the following key questions associated with the aforementioned coupling processes:

1. Why does the ionospheric disturbance often occur before strong earthquakes? How does this disturbance propagate from the lithosphere to the ionosphere or higher?
2. Could the electric field penetrate from thundercloud to the ionosphere and result to the electron density irregularities?
3. Could TLEs affect the profile of the electron density and the electric field in the ionosphere?

A possible space mission for the above key questions is illustrated in Figure 1.4. From the phenomena described above, the coupling processes between lithosphere and ionosphere are affected by the electric field greatly with different altitudes; therefore, an in-situ measurement of the electric field and plasma characteristics become important, especially for the initial phase of the coupling processes with different height. To satisfy this requirement, an elliptical orbit is chosen instead of a typical circular one to have an in-situ measurement covering different altitudes globally.

To study the electrical coupling process between the ionosphere, atmosphere and lithosphere, The AICE experiment is going to measure basic plasma parameters, electric and magnetic field in an elliptical orbit directly to explore the electrical coupling process between ionosphere and atmosphere, even lithosphere. This goal is achieved by the following scientific instruments: Electric Field Probe (EFP), Magnetometer (MAG), Te and Ne Probe (TeNeP), Ion Probe (IP), and Transient Luminous Event Imager and Photometer (TIP). The details of these instruments are described later.
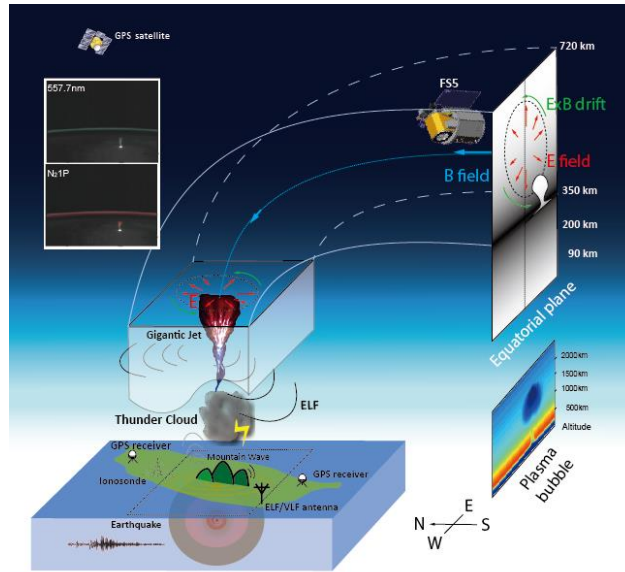
Figure 1.4 Sketch of electric coupling between the ionosphere and troposphere, or lithosphere. The earthquake, thundercloud or TLEs drive the electric field on the bottom of ionosphere, and then the plasma disturbance caused by electric field propagate along the magnetic field line to the equatorial region.

2. Design result

2.1.1 Orbital Analysis

The main objective of the AICE mission is to investigate the ionosphere-atmosphere coupling processes. Instead of a typical circular orbit, an elliptical orbit is chosen to achieve in-situ measurements from lower to higher altitude, and obtain the perturbation propagating along the vertical direction in the time scale of the orbital period. This elliptical orbit shaped with 300x700km is chosen and this orbit is also a critical challenge for the imaging.

An orbit with the low inclination angle is chosen to satisfy the following scientific requirements. First, the statistics from U. S. Geological Survey (Figure1.3) has already shown that most of the earthquakes with magnitude M greater than 5.0 occurred at low latitude (<45°), e.g. the Ring of Fire. Therefore, the anomaly of the electron density and temperature perturbed by earthquakes should congregate mostly in low latitude regions [Le et al., 2013]. Second, To observe the coupling process driven by thunderstorms, the low latitude regions, especially Intertropical Convergence Zone (ITCZ), with high rainfall and convection should be well covered. Third, the plasma irregularity enhanced by the coupling process of the earthquakes and thunderstorms can not be well identified by a polar orbit because the electron depletion parapagates along the magnetic field line. A low inclind angle orbit passing through diffrent magnetic field lines can help to recoganize this variation by comparing the electron densities in the longitudinal direction to locate the depletion.

The orbital parameters of AICE mission are shown in Table 2.1. The orbit simulation

renders the satellite coverage and the ground contacts as shown in Figure 2.1. The orbit period is about 95.7 minutes. Thus four ground contacts per day with an average contact duration of ~359 seconds are derived.

The plasma bubble and irrgularity in the ionosphere are mainly produced by the plasma instability and variate with seasons significantly. To identify the contribution from the atmosphere-ionosphere coupling process, a mission lifetime at least one year is necessary to eliminate the seasonal variation and to obtain sufficient samples for the statistics.

Table 2.1 Orbit parameter of AICE mission.

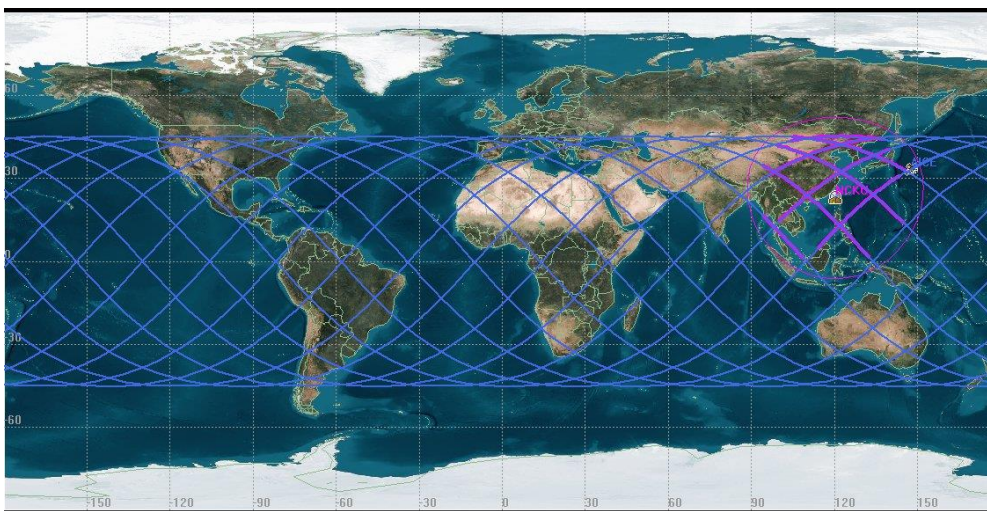| Apogee Altitude (km)	Perigee Altitude (km)	Inclination (degree)	Eccentricity	Orbit period (min)
700	300	45	0.029	95.7

Figure 2.1 The orbit projection of AICE on the earth.

2.1.2 AICE system

The AICE system consists of three segments, which are space segment, ground segment, and launch segment, respectively as depicted in Figure 2.2. The space segment is the AICE microsatellite which contains six subsystems and five scientific payloads. The ground segment is located in NCKU, which is mainly constructed and operated by NCKU team. The launch segment is the JAXA H-IIA launch vehicle in which AICE is expected to be launched in a piggy-back configuration.

There are six subsystems in the AICE microsatellite, including Structure and Mechanisms Subsystem (SMS), Thermal Control Subsystem (TCS), Attitude Determination and Control Subsystem (ADCS), Electrical and Power Subsystem (EPS), Telemetry and Tracking and Command subsystem (TT&C), and Command and Data Handling subsystem (C&DH). The five payloads, which are EFP, MAG, TIP, TeNeP, and IP are installed in the

AICE microsatellite. The system organization is shown as follows.

To conveniently install each circuit board of satellite subsystem and payload, the concept of modularized building block is realized in the AICE satellite configuration. This configuration provides modular design architecture to install devices in the microsatellite easily. The circuit board would be put in a 153mm x 153mm basic module, which is then fixed on the main frame of the satellite. There is a column frame, which can stack six subsystem modules, battery module, and fly wheel, on the center of the satellite. Then, the other scientific payloads, such as TIP, TeNeP and IP, would be fixed on side structure. Two kinds of mechanism to extend EFP are employed. One is attached on the top panel and deployed by the spin of satellite. Another one is fixed on top and bottom structure and extended by stepping motor. The deployment methods will be described later in Sec. 2.2.7.1. The four side panels of body (except top and bottom panel) are mounted with solar cells to catch sunlight power. Due to the S-band communication and photography requirement, S-band antenna and TIP are mounted on the side panel in nadir direction. The TeNeP and IP are equipped in the ram direction according to the scientific requirement.

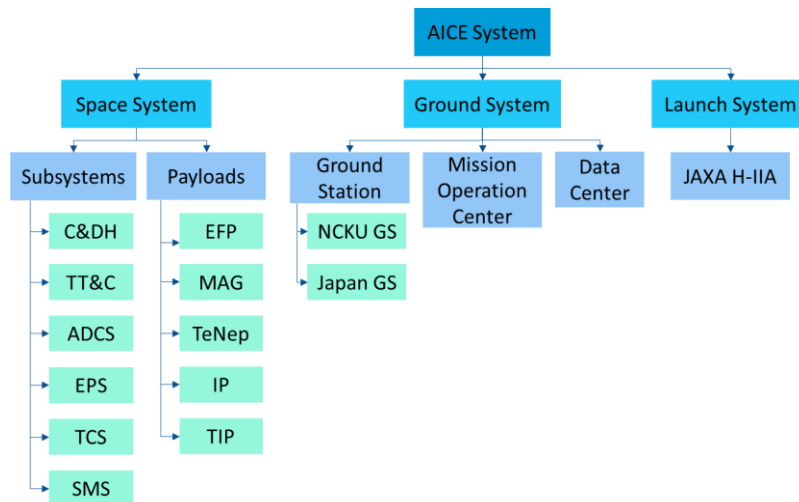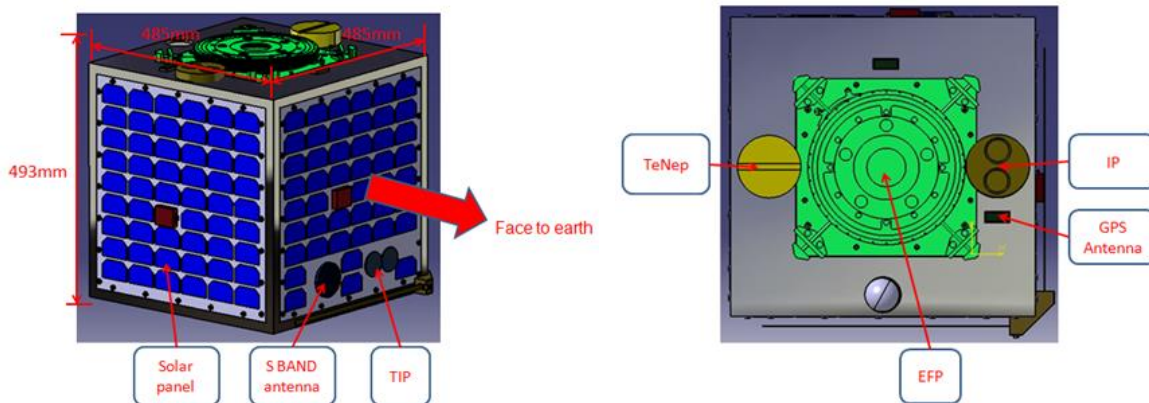*Figure 2.2* The AICE system overview.
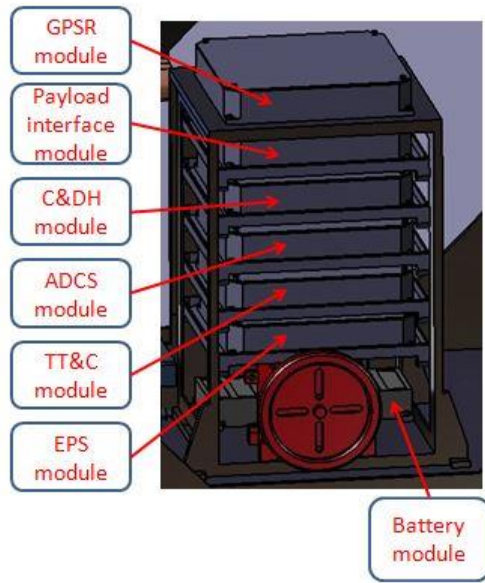

Figure 2.4 AICE Satellite Configurations.

Figure 2.6 AICE Satellite Inner Structure & module assignment.
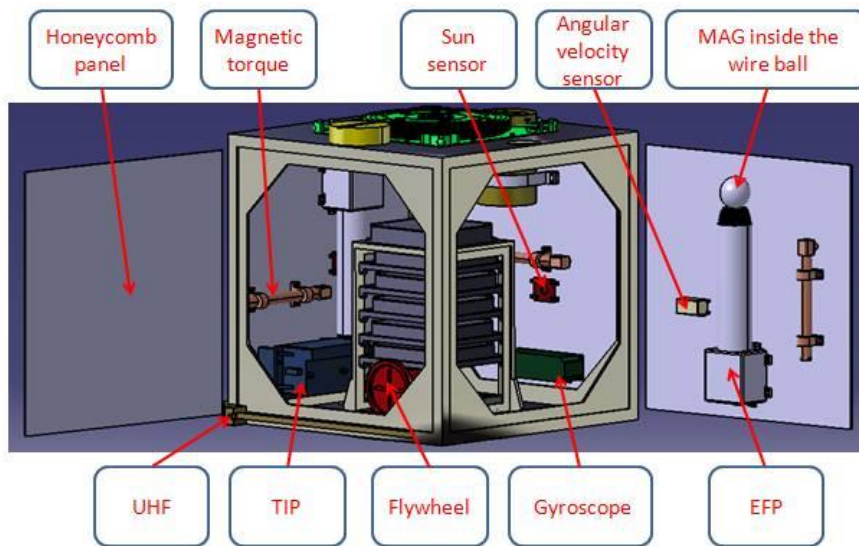

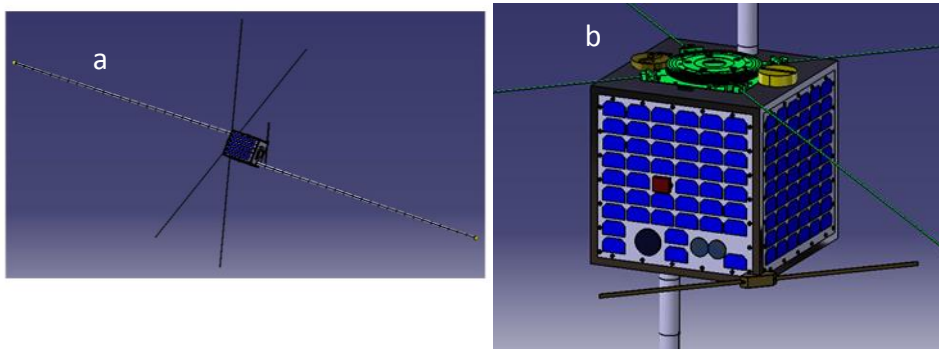*Figure 2.7* AICE Satellite Inner Configuration.

Figure 2.8 AICE Satellite Outer Configuration.

The electrical energy shall be provided by the surface mounted solar cells and the rechargeable batteries. The power budget of the AICE satellite is shown in Table 2.2. The total power consumption is about 58.71 W, and the available power is about 110.8 W according to the result of power generation analysis. So the solar cells can generate sufficient power for maintaining system operation. The dimension of AICE microsatellite is required to be 48.5 x 48.5 x 49.3 cm^3 and the mass is 45.84 kg. The mass budget of the AICE satellite is depicted in Table 2.3. The mass and configuration of the AICE satellite fulfill design constraints. The AICE communication will use amateur radio UHF band for telemetry and tele-command with data rate 9600bps as well as S-band with data rate 100 kbps for science data transmission. The link budgets are shown in the Table 2.4, Table 2.5 and Table 2.6. The inclination range is 1630 km.

Table 2.2 Power budget of AICE

Components		Power consumption (W)	
ADCS	Magnetic torques	0.85	1.45%
	Flywheel	23.8	40.54%
	Sensor	3.86	6.57%
C&DH		3.3	5.62%
EPS		1	1.70%
TCS		1.5	2.55%
TT&C	Transmitter	16	27.25%
	Receiver	3	5.11%
Subsystem		53.31	
TIP		3	5.11%
TeNeP		1	1.70%
IP		1	1.70%
EFP		0.2	0.34%
MAG		0.2	0.34%
Payload		5.4	
Total		58.71	100.00%
Average power generation		110.8	
Margin		47.01%	

Table 2.3 Mass budget of AICE

Components		Mass Allocation(kg)		Notes
SMS		20.24	44.15%	
ADCS	Magnetic torques	4.5	9.82%	
	Flywheel			
	Sensor			
C&DH		1.6	3.49%	
EPS		5	10.91%	Battery module included
TCS		1	2.18%	
TT&C	Transmitter	2.1	4.58%	S-band & UHF antenna included
	Receiver			
Payload Interface Board		1.6	3.49%	
Harness		1.3	2.84%	
Subsystem		36.84		
TIP		1.5	3.27%	
TeNeP		0.5	1.09%	
IP		1.5	3.27%	
EFP		4.5	9.82%	
MAG		0.5	1.09%	
Payload		9		
Total		45.84	100.00%	
Margin		8.32%		

Table 2.4 AICE communication frequencies and data rates

	Frequency Band		Path loss	Baudrate
Uplink	UHF	436.5MHz	152.08dB	9.6kbps
Downlink	UHF	436.5MHz	152.08dB	9.6kbps
	S-band	2.3GHz	166.51dB	100kbps

Table 2.5: Uplink and downlink budget for UHF

Parameter:	Value:	Units:
Ground Station:		
Transmitter Power Output:	10.00	watts
In dBW:	10.00	dBW
In dBm:	40.00	dBm
Transmission Line Losses:	-3.0	dB
Connector, Filter or In-Line Switch Losses:	-1.0	dB
Antenna Gain:	12.8	dBiC
Ground Station EIRP:	18.8	dBW
Uplink Path:		
Ground Station Antenna Pointing Loss:	-5.0	dB
Antenna Polarization Losses:	-3.0	dB
Path Loss:	-152.1	dB
Atmospheric Losses:	-0.5	dB
Ionospheric Losses:	-0.2	dB
Rain Losses:	0.0	dB
Isotropic Signal Level at Ground Station:	-141.98	dBW
Spacecraft:		
------ Eb/No ------		
Spacecraft Antenna Pointing Loss:	-3.0	dB
Spacecraft Antenna Gain:	2.2	dBiC
Spacecraft Transmission Line Losses:	-0.5	dB
Spacecraft LNA Noise Temperature:	66.8	K
Spacecraft Transmission Line Temp.:	290	K
Spacecraft Sky Temperature:	450	K
S/C Transmission Line Coefficient:	0.89	
Spacecraft Effective Noise Temperature:	499	K
Spacecraft Figure of Merit (G/T):	-25.3	dB/K
S/C Signal-to-Noise Power Density (S/No):	58.3	dBHz
System Desired Data Rate:	9600	bps
In dBHz:	39.8	dBHz
Telemetry System Eb/No:	18.5	dB
Telemetry System Required Bit Error Rate:	1.00E-05	
Telemetry System Required Eb/No:	9.7	dB
System Link Margin:	8.8	dB

Parameter:	Value:	Units:
Spacecraft:		
Transmitter Power Output:	1.0	watts
In dBW:	0.0	dBW
In dBm:	30.0	dBm
Transmission Line Losses:	-0.5	dB
Connector, Filter or In-Line Switch Losses:	-1.0	dB
Antenna Gain:	2.2	dBiC
Satellite EIRP:	0.7	dBW
Downlink Path:		
Satellite Antenna Pointing Loss:	-3.0	dB
Antenna Polarization Losses:	0.0	dB
Path Loss:	-152.08	dB
Atmospheric Losses:	-0.5	dB
Ionospheric Losses:	-0.2	dB
Rain Losses:	0.0	dB
Isotropic Signal Level at Ground Station:	-155.13	dBW
Ground Station:		
------ Eb/No ------		
Ground Station Antenna Pointing Loss:	-5.0	dB
Ground Station Antenna Gain:	12.80	dBiC
Ground Station Transmission Line Losses:	-1.10	dB
Ground Station LNA Noise Temperature:	169.6	K
Ground Station Transmission Line Temp.:	270	K
Ground Station Sky Temperature:	290	K
S/C Transmission Line Coefficient:	0.78	
Ground Station Effective Noise Temperature:	455	K
Ground Station Figure of Merit (G/T):	-14.9	dB/K
S/C Signal-to-Noise Power Density (S/No):	53.6	dBHz
System Desired Data Rate:	9600	bps
In dBHz:	39.8	dBHz
Telemetry System Eb/No:	13.8	dB
Telemetry System Required Bit Error Rate:	1.00E-05	
Telemetry System Required Eb/No:	9.7	dB
System Link Margin:	4.1	dB

Table 2.6: Downlink budget for S-band

Parameter:	Value:	Units:
Spacecraft:		
Transmitter Power Output:	1.0	watts
In dBW:	0.0	dBW
In dBm:	30.0	dBm
Transmission Line Losses:	-0.5	dB
Connector, Filter or In-Line Switch Losses:	-1.0	dB
Antenna Gain:	8.0	dBiC
Satellite EIRP:	7.0	dBW
Downlink Path:		
Satellite Antenna Pointing Loss:	-3.0	dB
Antenna Polarization Losses:	0.0	dB
Path Loss:	-166.51	dB
Atmospheric Losses:	-0.7	dB
Ionospheric Losses:	-0.1	dB
Rain Losses:	0.0	dB
Isotropic Signal Level at Ground Station:	-163.26	dBW
Ground Station:		
------ Eb/No ------		
Ground Station Antenna Pointing Loss:	-3.0	dB
Ground Station Antenna Gain:	30	dBiC
Ground Station Transmission Line Losses:	-0.5	dB
Ground Station LNA Noise Temperature:	92.3	K
Ground Station Transmission Line Temp.:	290	K
Ground Station Sky Temperature:	450	K
S/C Transmission Line Coefficient:	0.89	
Ground Station Effective Noise Temperature:	525	K
Ground Station Figure of Merit (G/T):	2.3	dB/K
S/C Signal-to-Noise Power Density (S/No):	64.6	dBHz
System Desired Data Rate:	100000	bps
In dBHz:	50.0	dBHz
Telemetry System Eb/No:	14.6	dB
Telemetry System Required Bit Error Rate:	1.00E-05	
Telemetry System Required Eb/No:	9.7	dB
System Link Margin:	4.9	dB

2.2 Satellite design
2.2.1 Structure and mechanisms subsystem (SMS)

In the structure design, the configuration and mass are designed to satisfy the limitations: dimensions should be controlled within 50 X 50 X 50 cm^3, the total weight of the satellite cannot exceed 50 kg. Because of the science requirement for EFP, the AICE mission extend 10 meter wire boom in 3 axial directions. Inside the main structure, a cuboids tower is built to stack the subsystems. The structure analysis is conducted to make sure the AICE survive during the launch and life cycle. The analysis process, shown in Figure 2.9, includes parameters setting, modeling, meshing, boundary conditions applying, solving and post-processing.
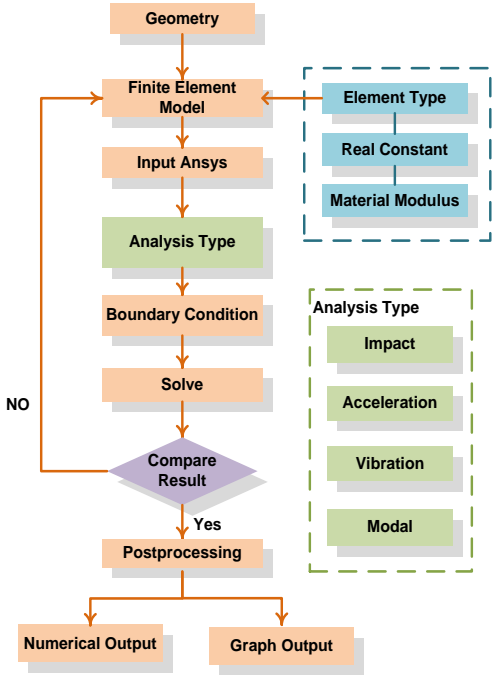

Figure 2.9 SMS Design Flowchart.

The modal analysis and random vibration analysis are performed to acess the structure deformation versus nature frequency. The vibration input power spectra are according to the specification of H-IIA launch rocket (Table 2.7, Asada et al.). The results are shown in Table 2.8. In addition to modal analysis, more analysis should be done according to the H-IIA launch vehicle parameter to make sure the AICE can satisfy the launch environment. The environment tests will be done to confirm the analysis result of AICE. The nature frequency of satellite and subsystem is regarding to be higher than 35 Hz. The first mode is 108.98 Hz, which satisfies the requirement of nature frequency.

Table 2.7 Input power spectra of vibration simulation

Quasi-Static Acceleration

	Longitudinal	Lateral
Compression	-6 G	$\pm$ 5 G
Tension	5 G	$\pm$ 5 G

Sine Wave Vibration

	Frequency(Hz)	Acceleration
Longitudinal	5-100	2.5 G
Lateral	5-100	2 G

Random Vibration

Frequency Width(Hz)	Acceleration (G^2/Hz)
20-200	+3 (dB/octave)
200-2000	0.032
Actual	7.8 (Grms)

Table 2.8 Modes versus Frequency

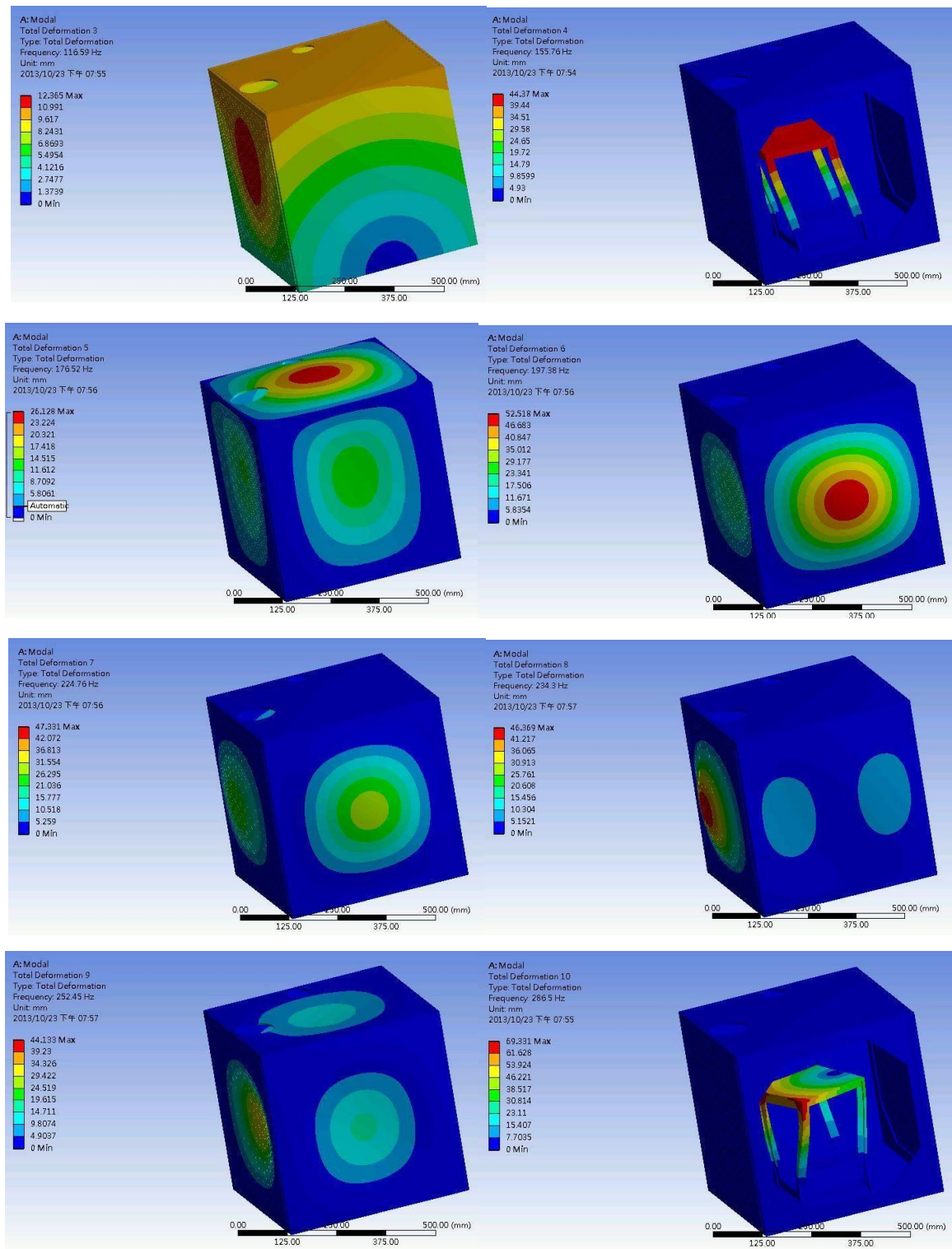| Mode	Frequency(Hz)
1	108.98
2	112.53
3	116.59
4	155.76
5	176.52
6	197.38
7	224.76
8	234.3
9	252.45
10	286.5
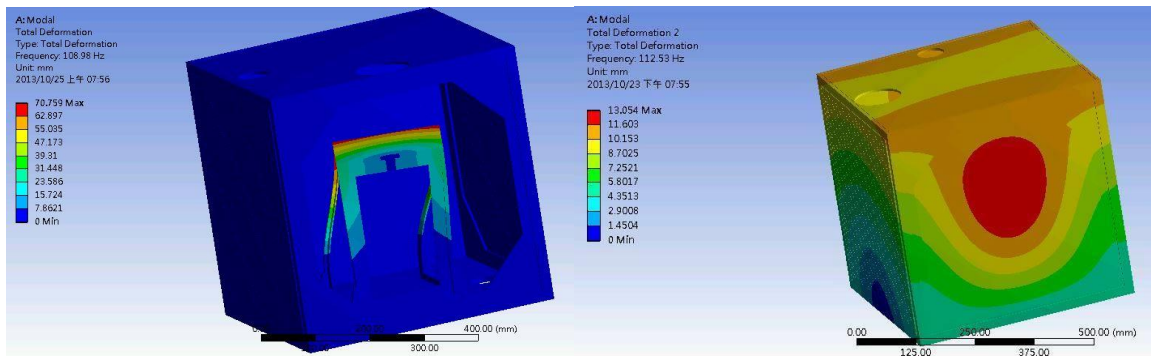
Figure 2.10 Nature frequency modes.

2.2.2 Thermal control subsystem (TCS)

The AICE thermal control is basically a passive design. However, active thermal devices, heaters or cooling devices will be employed while temperature of any component out of the tolerance range. In the TCS analysis flowchart, team members will obtain orbit information, simulate heat flux, build satellite thermal model, and determine the radiation exchange factors

and view factors to obtain the thermal simulation results. Passive thermal control will be adopted according to thermal analysis results, for examples, providing appropriate thermal insulation and selecting the proper material properties.

Our design uses anodizing process on the satellite structure and panel. Because one side of AICE is always pointing to the earth and the heat flux of this side from the sun is less than the others, so this side are subjected to black anodized process for increasing the absorptivity and increase the temperature by absorb the radiation from the earth. This, in turn, will make this satellite in a temperature uniform condition. In contrast, the other outer sides are subject to anodized process. The inner sides of the satellite structure are coated by Kapton to slightly increase the absorptivity, so the inner side of the panel can keep the heat coming from the battery module and C&DH module, the Kapton coating is chosen to minimize the temperature fluctuation inside the satellite.

.

Table 2.9 anodizing process

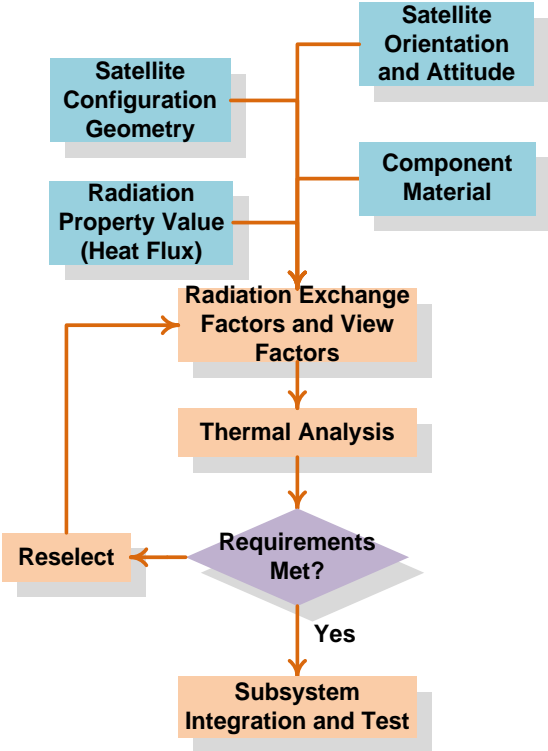| Item	Material	Coating	α (Solar)	ε (IR)
Panel		Kapton	0.42	0.78
	Al 6061	Anodized	0.3	0.76
Frame		Black Anodized	0.67	0.87
Solar Cells			0.68*	0.895

Figure 2.11 TCS Analysis Flowchart.

Considering the AICE configuration, orbit and attitude, the preliminary thermal analysis is executed. The coldest case (as shown in Figure 2.12) is zero β angle (the angle between the orbital plane and the sunlight) and the satellite go through earth's shadow mostly. The hottest case is 87 degree of β angle and the satellite is irradiated by sunlight mostly. Table 2.10 shows the coldest and hottest case of panels and modules, which shows AICE can sustain and operate in space environment. In the future, the AICE should also do the environment test to confirm the analysis result.
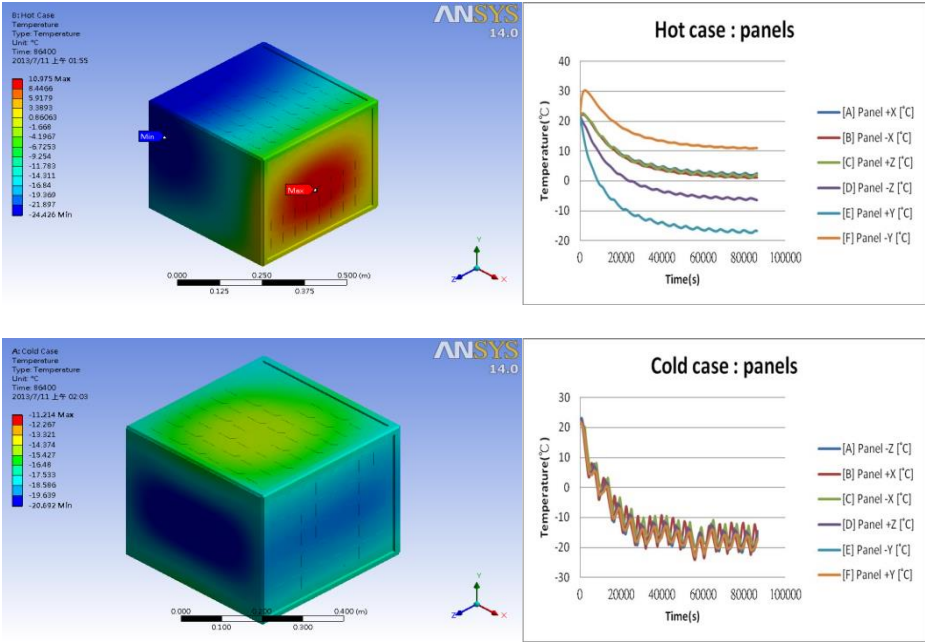

Figure 2.12 Hot case and Cold case of panels.

Table 2.10 temperature table

	Hot case(℃)	Cold case(℃)
Panel +X	2.4626	-16.083
Panel –X	1.1951	-16.265
Panel +Y	-16.704	-17.025
Panel –Y	10.955	-17.222
Panel +Z	1.8556	-15.326
Panel –Z	-6.3122	-14.615
EPS	-6.1117	-14.738
GPSR	-3.947	-11.505
Battery	-10.835	-18.009
C&DH	-1.7476	-11.214
TT&C	-3.0404	-12.641
ADCS	-1.7993	-11.589

2.2.3 Attitude determination and control subsystem (ADCS)

There are two important requirements for attitude determination and control system. One is the stabilization task, when the satellite deploys the EFP. Because the each electric field probe is about 5 m and end with a metal spherical probe, the moment of inertia will be increased after probes are completely extended.

Another task is satellite attitude control for imaging. The camera must always aim nadir direction for the observation of Transient Luminous Events, so the satellite has to conduct attitude control accurately in elliptical orbit. To conquer these two tasks, a fly wheel and a three axis magnetic torques are employed. Additionally, attitude sensors are equipped to provide attitude imformation, as listed in Table 2.11.

The ADCS consists of a three-axis magnetometer, gyroscope, sun sensor, and GPS receiver. Then, the satellite position and attitude could be determined through these measurements. Three-axis magnetic torque rods and flywheels are employed for satellite stabilize or adjusting attitude for mission operation. An onboard processor (32-bit ARM or MCU) executes the attitude software and interfaces with the sensors and actuators via the ADCS interface board. The ADCS architecture is shown in Figure 2.13.

In the beginning of ADCS design, choosing proper satellite and environment models in simulation will be conducted to verify the feasibility and obtain pertinent design parameters. The system specification and requirements are established by the information. Then, the Software-In-the-Loop (SIL) test, extensive simulations, is conducted to verify the attitude control operation through the control algorithm, attitude filters, sensor models, actuator models, and mode switching logics. After that, the hardware platform for real time control will be prepared, designed, and implemented. Afterward, the Processor-In-the-Loop (PIL) is used to verify ADCS hardware and software before the ADCS is integrated into the satellite.

After satellite separation from launcher, the AICE will perform the B-dot control for satellite detumbling. From the requirements of the satellite communication pointing and photography, the AICE employs three-axis attitude controls by means of flywheels. Therefore, the AICE ADCS should be also controlled against external disturbances. After the detumbling mode, the AICE will perform the attitude determination via an Extended Kalman Filter (EKF) to supply input for the three-axis stabilization control laws. The AICE will implement the momentum biased stabilization for executing the three-axis stabilization control laws.
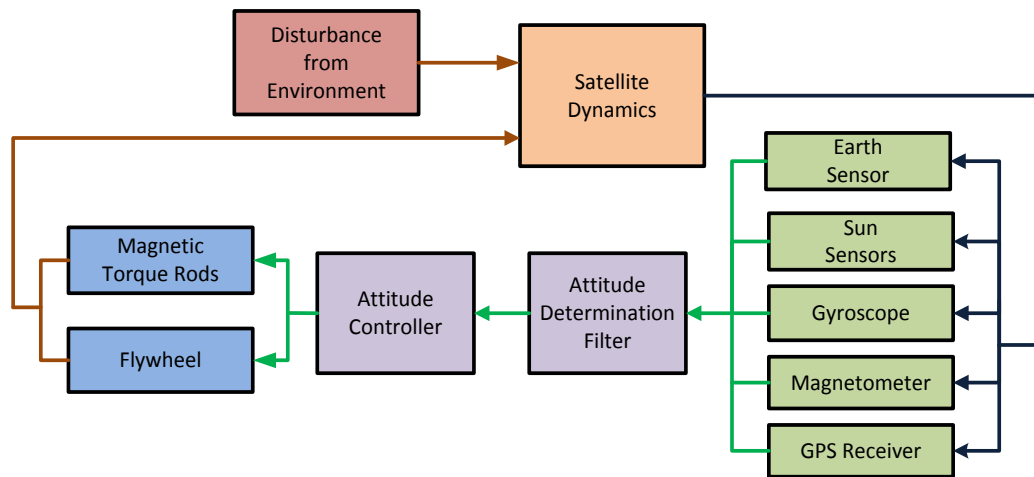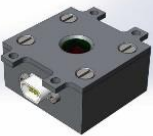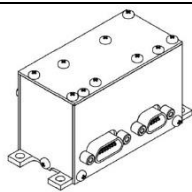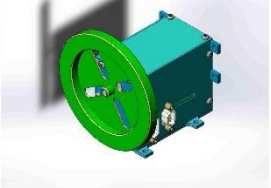
Figure 2.13 The ADCS architecture of AICE.

Table 2.11 Sensors/Actuators

Sensors	Sun sensor	Gyroscope
Feature		
Measurement range	$\pm 60°$	$\pm 250°/s$
Noise	Less than$\pm 0.1°$	up to $\pm 0.005°/s$
Power consumption	0.05 W	1.2 W
Mass	100 g	90 g
Dimensions	18x46x38 mm	34x38x66 mm
Operating temperature	-40..+100 ℃	-40..+60 ℃

Sensors	Earth sensor
Feature	
Dip angle measurement accuracy	0.1°
2-axis attitude accuracy	0.5°
Weight	85g
Power consumption	0.36W
Operation temperature	-40 to +80℃

Actuator	Magnetic torques	Flywheel
Feature		
Maximum magnetic moment	5 A·m²	
Maximum angular momentum		0.25 Nms
Maximum power consumption	0.85 W	23.8 W
Mass	200 g	300 g
Dimensions	330 mm, Ø 10 mm	84x86x71 mm
Operating temperature	-40..+80 ℃	-40..+80 ℃

2.2.4 Electrical power subsystem (EPS)

The EPS shall generate, store, regulate and distribute the electrical energy for the subsystems and the payloads during all phases of operations. The EPS is composed by the Power Distribution and Regulation Unit (PDRU), the battery pack, and the solar cells. The PDRU is used to regulate voltage (3.3 Volt, 5 Volt, or 7 Volt, etc.) and distribute power to each subsystem and payload. Moreover, the PDRU has onboard microcontroller which can measure the bus voltages, currents, and battery status automatically, and send the data to C&DH. The rechargeable batteries are used to store sufficient energy for satellite peak power demands and eclipse periods. The battery pack will be connected with a protection circuit against power failures, such as over-charge protection, over-discharge protection, and short-circuit protection. The power of satellite is generated by solar cells during sunlight. The overall schematic of the EPS is illustrated in the following Figure.
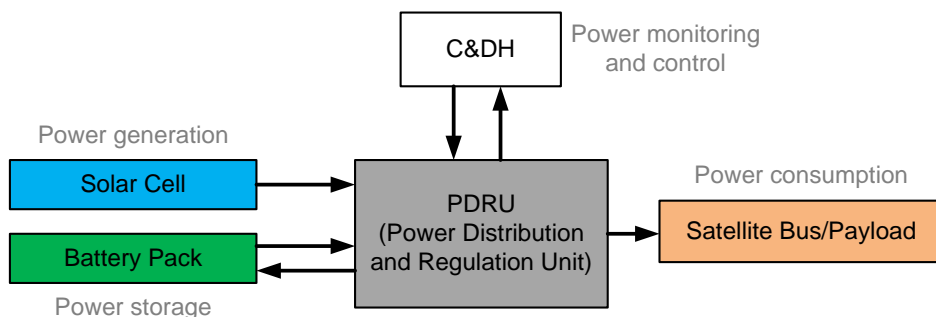

Figure 2.14 The EPS architecture of AICE.

2.2.5 Commend and data handling subsystem (C&DH)

C&DH is the heart of a satellite, it is in charge of command validation and execution, data reception, store and downlink, and maintain satellite in health. C&DH is also the interface for managing the communication of subsystems and payloads. Every payloads have its own data

handling electronics (control board), C&DH is the leader who send I2C messages to the control board. The control boards receive I2C messages and decode it, then run proper actions according to a pre-set table. The C&DH controls the on/off status of payloads and collects the science package from control board.

The on-board data handling equips an ARM7 32-bit RISC processor with low power consumption and excellent performance. I2C provide a convenient interface to communicate with each subsystem. It helps us easily add or remove payloads & bus, making it more convenient to build a modular system. And the RTC (real time clock) frees system from time-critical tasks, and it is more accurate. (Figure2.15)

The onboard flight software is mainly assembled by three Components: House Keeping Component(HKC),Data Collection Component(DCC) and Communication & Command Component (C&CC). The onboard flight software is a modular design, mainly assembled by three components: House Keeping Component (HKC), Data Collection Component (DCC) and Communication & Command Component (C&CC). Components are the logic grouping of modules, performing common functions and purpose. Each component contains two to four module units, like ADCS Module, Up&Downlink Module, Reboot Module, and etc. These three components will be put into a Loop-while of main function so that the program will externally switch between them.
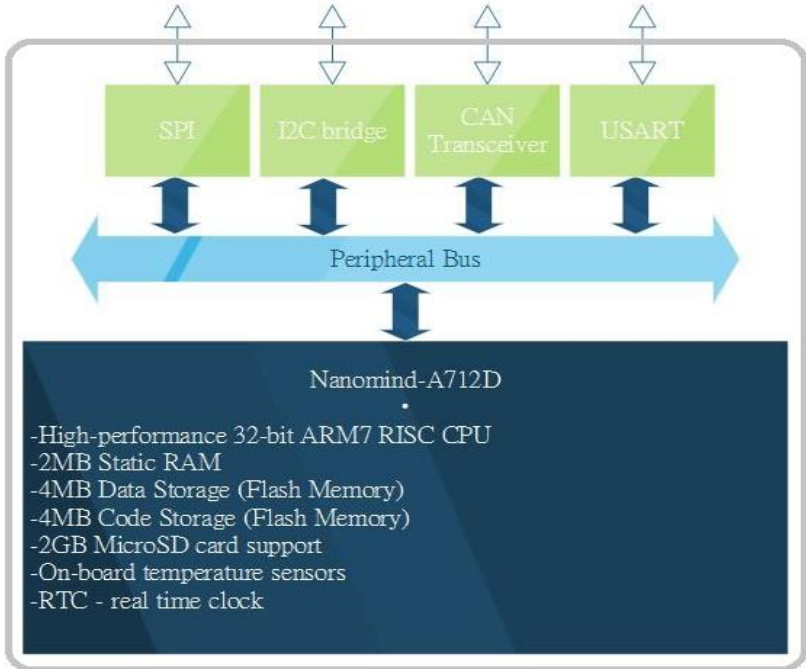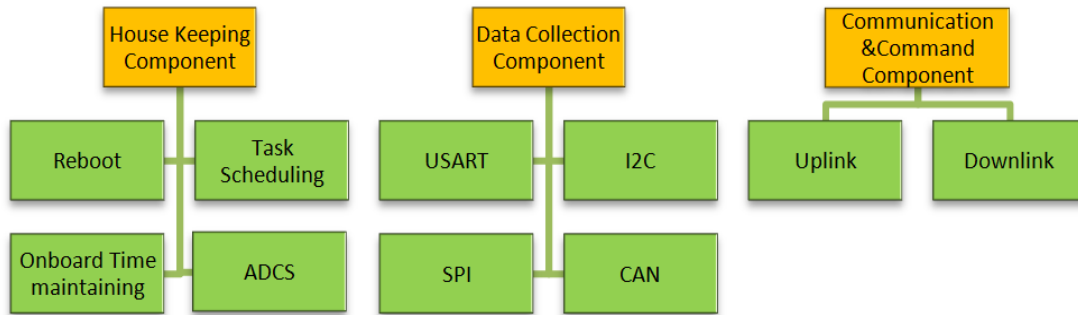

Figure 2.15 C&DH Block Diagram

Figure 2.16 Flight Software structure

2.2.6 Telemetry, Tracking and Command subsystem (TT&C)

The satellite communicates with the ground station through the TT&C subsystem through two bands: UHF amateur radio band and S-band. The UHF amateur radio band are used to perform beacon broadcasting, telemetry downlink, and telecommand uplink. Additionally, the S-band is adopted for the higher downlink rate. The TT&C will send a periodic Morse beacon for satellite tracking and verify house-keeping data. CCSDS connection oriented telemetry protocol will be implemented to keep a reliable connection. The TT&C operation procedure is proposed as follows: TT&C system will be constantly waiting for ground station commands. It will also send a periodic signal of the satellite status. The scientific data is transmitted through S-band. A detailed operation of the communication process is given in Figure 2.17.

The data generation per day is estimated in Table 2.12. The EFP, MAG, TeNeP and IP, sample 2 Hz, and a time and place tag are attached before each measurement. To keep a proper formatting for the storage of data, the following types of frames are designed to identify the type of data as well as its content:

a) Mission Frame: This frame contains the complete scientific measurements of the project.

b) Quaternion Frame: Contains quaternions data that will be used for attitude determination

c) SOH Frame: Contains the State of Health of the satellite

d) Reference time tag frame: Contains a precise reference of time.

The definition of each frame are defined in Table 2.13.

Using this reference of frames, the daily data generation is estimated by assigning the active period, which is about 81 Mbits per day. Considering the downlink rate of S-band is 100kbps, and approximately 15 minutes per day for communication. Assuming, 70% of download time usage; 100 Mbits of data per day could be download. The currently expectation for scientific data without TIP is about 81 Mbits, and the rest is planned to be used for images and photometer data taken from the TIP. This is shown in the Table 2.14.
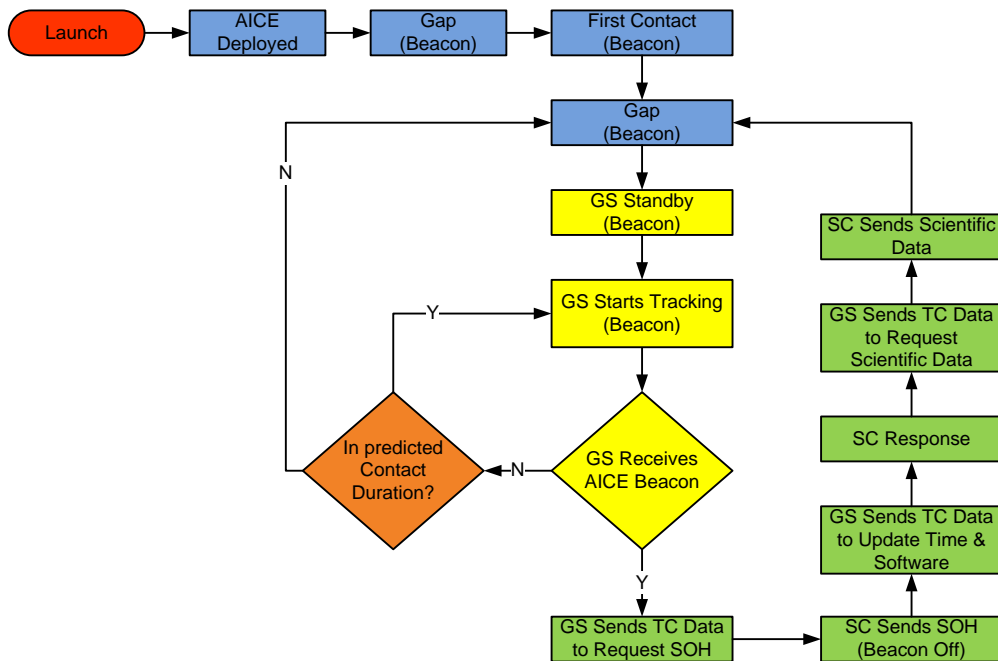
Figure 2.17 Communication flow chart of AICE

Table 2.12 Science data generation of AICE

	Period (s)	Number of measurement	Resolution (bit)
EFP	0.5	3	16
MAG	0.5	3	16
TeNeP	0.5	2	12
IP	1	100	12

Table 2.13 Frame definition

a)	ID	Time Tag	GPS Tag	EFP		Magnetometer		TeNeP		IP
	8	16	72	36	36	36	36	24	24	600

b)	ID	Time Tag	GPS Tag	Quaternions			
	8	80	72	64	64	64	64

c)	ID	Time Tag	GPS Tag	SOH
	8	80	72	2048

d)	ID	Time Tag
	8	24

Table 2.14 Daily data generation

Package generation Period (s)	Bits	Active hours	Total amount of data (bits)
1	888	24	76723200
30	416	24	1198080
30	2208	24	6359040
1	32	12	1382400
Data daily generation			85662720

2.2.7 Payload

The goal of this mission is to measure the plasma variation caused by the disturbance of the ambient electromagnetic fields which is possibly driven by earthquakes or thunderstorms. The electromagnetic field measurements are done by a 3-axes Magnetometer, and a 3-axes Electric Field Probe. Furthermore, the Ion Probe is used to obtain the ion flow, relative ion density, and ion temperature. The Te and Ne Probe is designed to acquire the electron density and temperature. To register the activities of the energetic lightening, the Transient Luminous Event Imager and Photometer are installed in the nadir direction. The details of these scientific instruments are described below.

2.2.7.1 Electric Field Probes (EFP)

In the AICE mission, the most important and fundamental parameter is the electric field in ionosphere which may be disturbed by the electric coupling process from the troposphere or lithosphere. The electric field measurement by double spherical probes is a widely used in the space mission [Paschmann et al., 1998]. It is firstly placed onboard the S3-3 spacecraft in 1976 [Mozer et al., 1979]. Thus the electric field in the direction of the boom is determined by the distance separation and potentital difference which is measured by the double probes. However, the electromotive force caused by the velocity of the spacecraft across the magnetic field lines should be corrected necessarily [Maynard, 1998]. The EFP can measure the accurate electric field directly in all directions insetad of an indirect derivation by th $\vec{E} \times \vec{B}$ drift of the ion or electron.

The typical electric field in ionosphere ranges from a few tens mV/m to a few hundreds mV/m. To amplify the signal, the probes have to extend to 5 m apart from the spacecraft with identical conducting spheres on the end of wire boom. The specifications of EFP are shown in Table 2.15. A passive wire boom deployment system is engaged in two axes which have been successful deployed in the DICE mission (2009) for a two-axes measurement of the electric field. The probes are bended into a wheel as their storage position before launch. After

De-tumbling of the satellite, the wire booms are deployed by cutting a latch wire and extend by the spin of the spacecraft. The third axis of probes is extended by the stepping motors. The schematic drawings are shown in Figure 2.18 and Figure 2.19. Furthermore, Figure 2.20 demonstrates a one-axis double spherial electric field probe in a balloon experiment carried out in Taiwan.
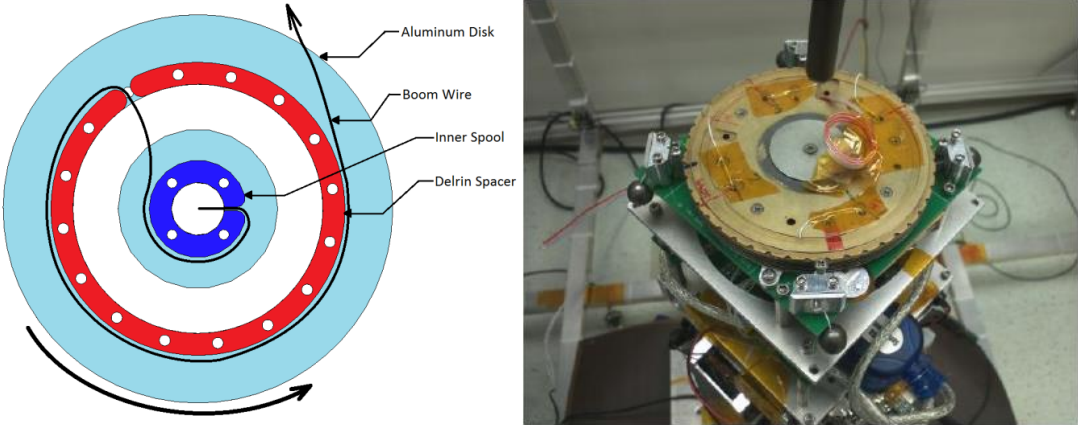

Figure 2.18 Miniature Wire Boom System for the Cubsat Application, Keith R. Bradford, *Utah State University*
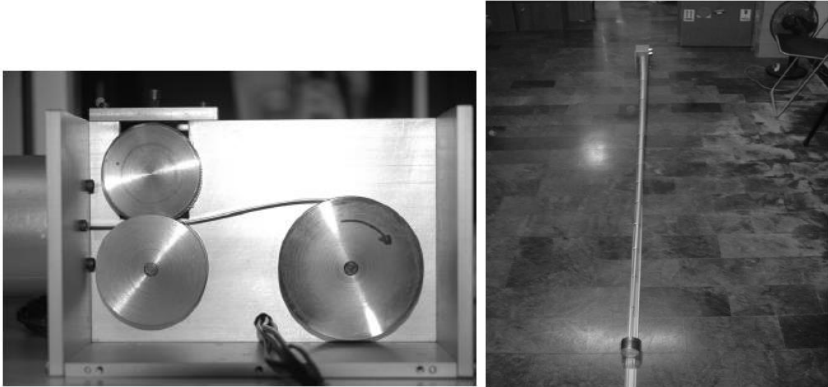

Figure 2.19 The design of a low-cost gravity gradient boom for microsat, [Hong et al., 2007]

Table2.15 Major Specifications of the EFP

Dynamic Range	+/-10V
Electric Field Resolution	~16μV/m
Power consumption	< 200 mW
Mass	300 g (TBR)
Dimension	25 x 25 x 2 (cm) (TBD), 10 m tip to tip
Sampling Rate	2 Hz (TBD)

Figure.2.20 One-axis double sphere electric field probe for balloon experiment.

2.2.7.2 Magnetometer (MAG)

In addition to the electric field, the magnetic field also drives the motions of the plasma in the ionosphere via $\vec{E} \times \vec{B}$ drift. The study on the Dst index shows that the background geomagnetic field, ~65,000nT, varies from a few to hundreds of nT. Commercial products of the HMC 101 and 1021 sensors manufactured by Honeywell are used to build a 3-axis magnetometer for the AICE mission. The sensors utilize Anisotropic Magneto-Resistive (AMR) material with high sensitivity and compact, comparing with the search-coil type magnetometer. The MAG is small enough to mount inside one of the sphere of the electric field probe. The dynamic range of MAG covers from a few nT to ~600,000 nT. The specifications of the MAG is listed in Table 2.16. Figure 2.21 shows a MAG manufactured by NCKU and installed onboard the Taiwanese sounding rocket.

Table2.16 Major Specifications of the MAG

Range	±600,000 nT
Accuracy	0.85 nT
size	42 x 32 x 20 mm
Mass	35 g (harness included)
Power Consumption	< 200 mW
Sampling rate	2 Hz

Figure 2.21 the MAG onboard the Taiwanese sounding rocket.

2.2.7..3 Electron temperature and electron density probe (TeNeP)

The TeNeP measures the electron temperature and electron density by integrating the instruments of the eletron temperature probe (ETP) and planar impedance probe (PIP). The electron temperature and density can be measured alternatively by switching the operation mode of the ETP and PIP. The TeNeP system is very compact, light weight and low power consumption, and is able to have accurate measurements on the electron temperature and density. The background plasma density ranges about 10^9 to 10^{12} e$^-$/m^3 derived by IRI-2007 model at the AICE mission altitude. Therefore, the specifications of the TeNeP listed in Table 2.17 confirm that the current design can satisfy the requirement.

Figure 2.22 Picture of TeNeP.

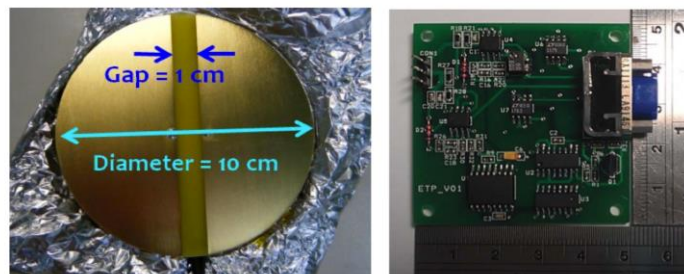*Table 2.17* Major Specifications of the TeNeP

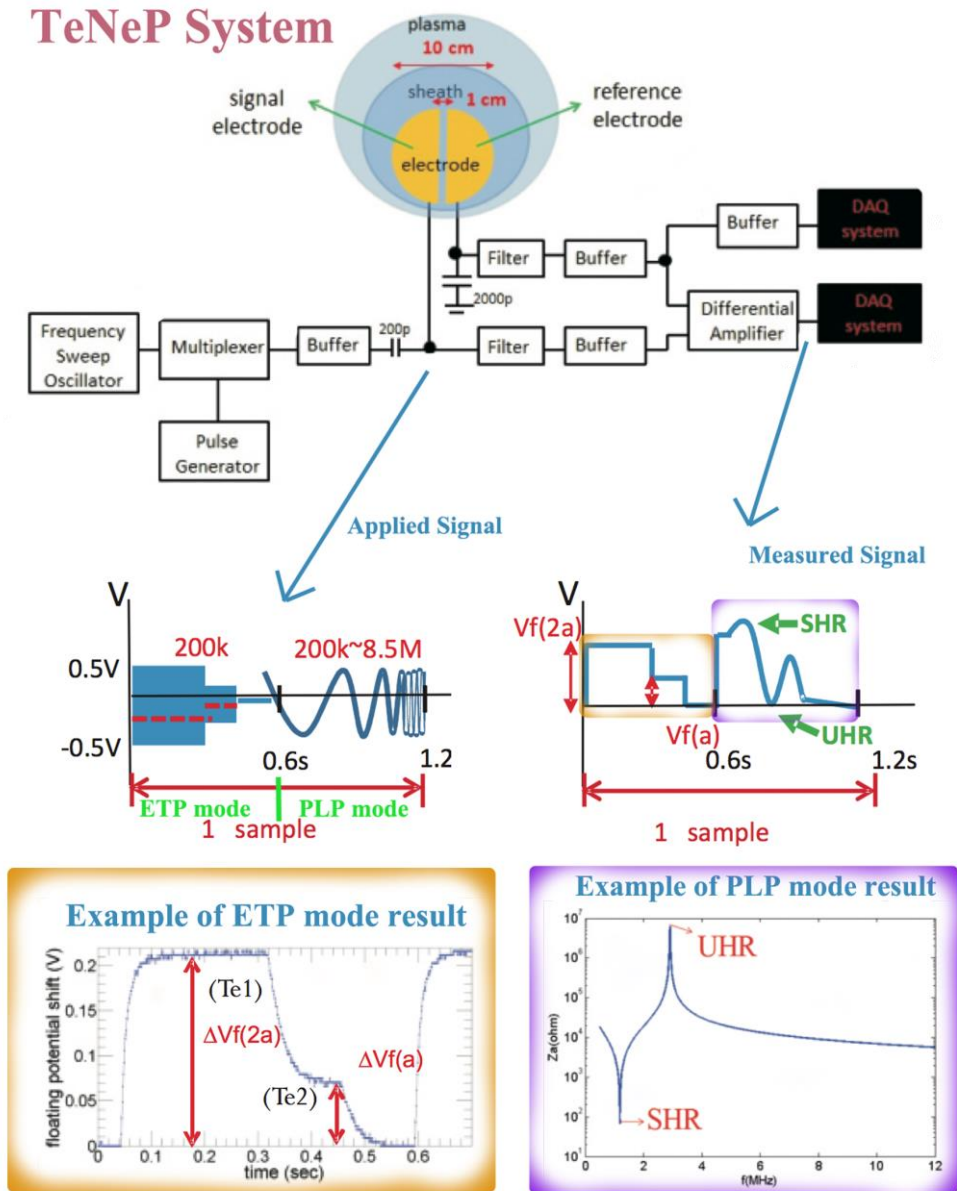| Range	T_e: 1000-3000 K N_e: 10^9-10^{12} m^{-3}
Accuracy	15%
Power Consumption	< 1W
Size	10 (Dia.) x 3 (H) cm
Weight	250g
Sampling rate	2 Hz

Figure 2.23 TeNeP system and examples of measurement results.

The operation modes of ETP and PIP are implemented for the TeNeP (Figure 2.23). In ETP mode, RF sinusoidal signals (200 kHz) of two different amplitudes, "a" and "2a" in Figure 2.23, are applied on the TeNeP. The two levels of DC voltage output arise from the probe floating shift under RF signal of two amplitudes. Then electron temperature is derived from the ratio of output DC voltage levels accordingly.

In PIP mode, the TeNeP transmits electro-dynamic waves to the plasma to find the Upper Hybrid Resonance (UHR) by sweeping a wide range of frequencies (200kHz – 8.5MHz). Due to the characteristics of PIP mode, the TeNeP get rid of the electrode contamination problem and can provide high accuracy of electron density measurement.

2.2.7.4 Ion probe (IP)

The Ion Probe (IP) consists of two units for the ion measurements (as shown in Figure 2.24): Retarding Potential Analyzer (RPA) and Ion Drift Meter (IDM). Therefore, IP is capable to measure te ion temperature, composition and the relative densities of individual ion species by the RPA unit, and also obtain the ion drift vector by the IDM unit simultaneously.

The RPA unit is composed of six metal grid meshes and one collector. A schematic figure is shown in Figure 2.25. A biased mesh repels the incoming electrons out and a sweeping voltage is applied on another meshes for the ion energy selection. The ions passing through all grid meshes are collected by the collector. The structure of the IDM unit is similar to the RPA. However the collector of the IDM unit is replaced by the configuration of 2 x 2 plates instead a single one. Comparing the ion currents collected by the plates, the ion drift vector including velocity and direction is derived directly. The specifications of the IP are shown in Table 2.14.
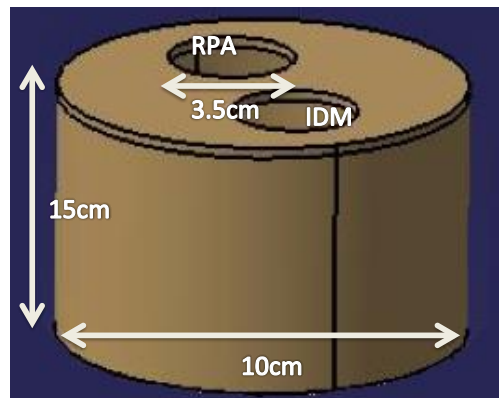

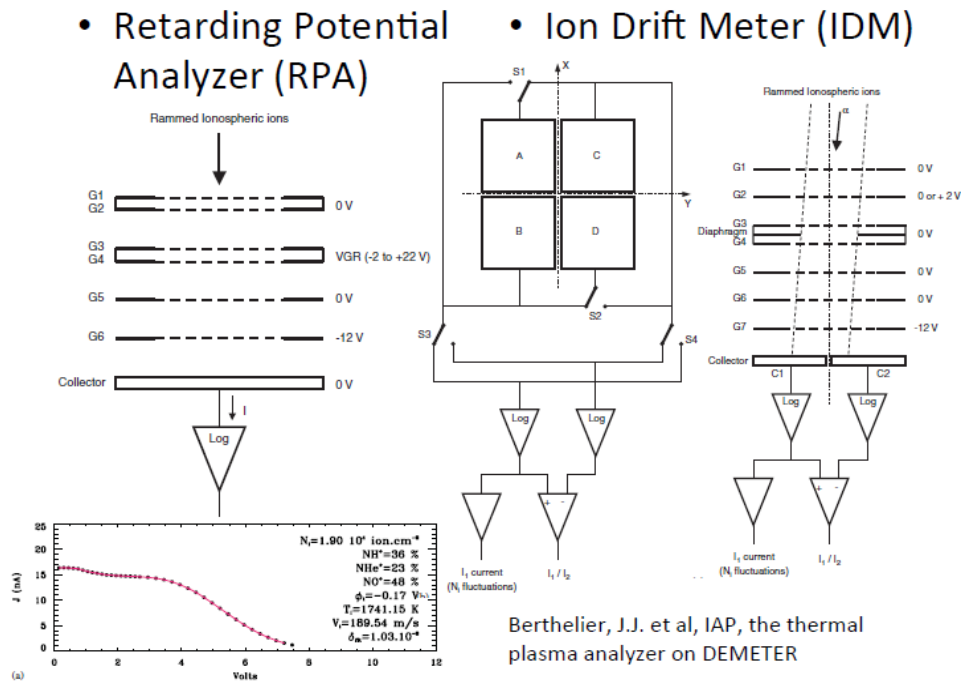
Figure 2.24 Dimension of Ion Probe

Figure 2.25 The schematic diagrams of the IP including the RPA and IDM units

Table 2.14 Major Specifications of the Ion Probe

Range	N_i:10^8-10^{12} m^{-3} E_i: 0-22 eV V_i:0 -6 km/s
Accuracy	15%
Power	< 1W
Size	10 (Dia.) x 15 (H) cm
Weight	1.5kg
Data rate	1 Hz (TBD)

2.2.7.5 Transient Luminous Event Imager and Photometer

TLEs are identified to be triggered by intense lightening, therefore a measurement to the intense, not general, lightning can help to catch the short interaction driven by TLEs. The Transient Luminous Event Imager and Photometer, includes a micro camera and a photometer, is used to record TLEs and this instrument is the heritage of the ISUAL instrument on-board FORMOSAT-2 and new innovation by NCKU team.

2.2.7.5.1 Micro camera

A compact size, high sensitivity micro camera is employed to record TLEs (Figure 2.26). A commercial lens of Moritex ML-1214 (12mm, F/1.4) is installed to have a FOV of 22.0 X 16.5 degree. Also, the CCD is Commercial-Off-The-Shelf (COTS) grade. A bandpass of 623-750nm ((N$_2$ 1PG)) is chosen to have a best efficiency on the TLE detections. The power consumption of this micro camera is very low, and 500mW of orbital average is expected. The camera takes images with a rate of 30 frames per second to a circular buffer continuously, and saves to the mass memory when the photometer is triggered by the intense lightning or TLEs. By this observation mode, only certain transients are captured by the optical instrument set. Usually, the images takes lots of downlink band, to shrink the data volume, a standard, lossless, data compression algorithm JPEG-LS is implemented inside. The specification of the micro camera can be saw from Table 2.14.

Table 2.14 Major Specifications of the Micro Camera

Bandpass	623-750nm (N$_2$ 1PG)
Optics	12mm, F/1.4
FOV	22.0 X 16.5 degree
Detector	E2V CCD97 EMCCD
Effective gain	~3000
Mass	500 g
Size	65 X 70 X 130 mm^3
Power	< 500 mW (TBR)

Figure 2.26 Picture of Micro Camera (DOTCam) for Japanese microsat RISESAT mission.

2.2.7.5.2 Photometer

There are another N$_2$ 1st Positive band emission sources in the night time. To screen out the fault trigger, N$_2$ LBH band (150-280nm) is detected by a high sensitivity photometer. The N$_2$ LBH emission is an important and unique signature of the TLEs [Chang, 2010] because

the N_2 LBN emitted from lower atmosphere such lightning photon will be absorbed by the atmosphere, and only the emission in the upper atmosphere will be detected from space. Unfortunately this emission is mainly locating on Near-UV band and cannot be detected by CCD-based imager. Instead of CCD camera, a sensitive photon multiplier based photometer is equipped to detect this interesting N_2 LBH emission.

The photometer is a heritage of the ISUAL. The field of view is the same as micro camera. After powered on, this photometer continuously records data with a sampling rate of 10k Hz to a circular buffer and process by an on-board processor. When the signal variation exceeds a pre-programmed trigger criteria, all data in the circular buffer is be stored to the mass memory, and generate a interrupt to the micro camera to store data. The spec. is shown in the following table.

Table 2.16 Major Specifications of the photometer.

Bandpass	150-280nm (N_2 LBH)
Optics	12mm, F/1.4
FOV	22.0 X 16.5 degree
Detector	Hamamatsu R7400-09
Sensitivity@ SNR=10	0.1E-6 W/m2
Mass	~1kg
Size	70 X 60 X 130 mm^3
Power	>2W(TBR)

2.3 Ground segment
2.3.1 Ground station

The basic role of ground stations is to communicate with satellites including upload commands and download telemetry. Generally, ground station consists of six subsystems as below: antenna subsystem, transmitter subsystem, receiver subsystem, terminal subsystem, communication monitoring subsystem and power subsystem. There are two ground stations that will be used in the operation of AICE, one of them is in ground station of NCKU and the other is located at Japan Earth Observation Center (EOC). The NCKU Ground Station (GS) will be equipped with an S-Band antenna and a set of UHF antennas. It will be used as a primary ground station site which can send commands and recover SOH data and scientific data. It is located at 22°56'17''N 120°16'38''E and 31 meters height from sea level.

The station at Japan Earth Observation Center (EOC) is also considered for the collection of science data as a secondary station. EOC station is located at 36°0'10.99''N 139°20'56.83'' and its height is 581 meters.

2.3.2 Mission operations system

GS uplink commands to the satellite and receive the scientific data and SOH (Status Of Health) from the satellite. The responsibility of the Mission Operations center (MOC) is to keep the satellite in healthy condition and carry out operations to achieve the mission objectives. The MOC would support analysis of the satellite's health status from satellite telemetry, update and synchronize the onboard time, payload experimental task scheduling. The MOC will also preserve all mission documents for trouble shooting and further satellite design reference. Mission operation control is to deal with the data from the satellite and monitor the condition, also to store data and control s-band.

2.3.3 Data distribution

Data distribution is to manipulate the scientific and SOH data after getting them from the AICE satellite. After the data is downloaded by ground station, it is sent and stored to the data distribution center in time. The major tasks of data distribution center are to unpack the level-0 data, carry out calibration and necessary processing. The SOH is also monitored by the data distribution center to identify potential problems and report to associated staff if necessary. The final products of the scientific and SOH data are opened to the scientific community and engineering team respectively for further analysis and application.

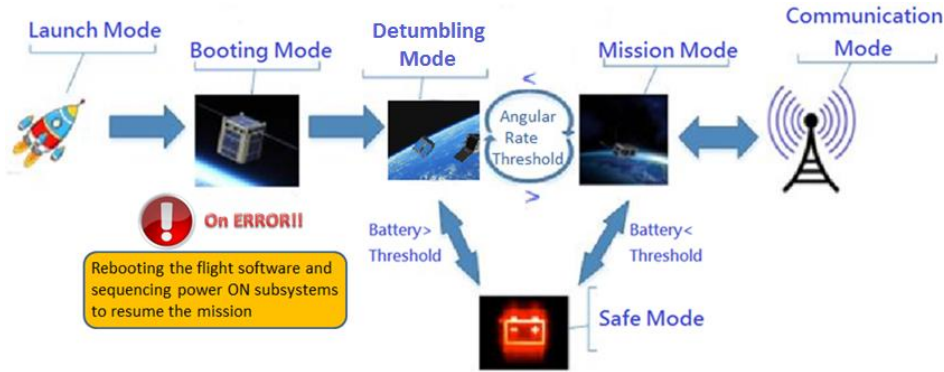## 2.4 Operational procedures

Figure2.27 Operation Modes of AICE

The following operation modes are implemented, including Launch mode, Booting mode, Detumbling mode, Mission mode, Communication mode, Safe mode and Error Detect Report (EDR) (see Figure 2.27). Before launching, the satellite is powered off and storage in the launcher. After the satellite separates from the launcher, the main power bus gets the power from batteries and solar array to initiate and reboot the flight software. The satellite transfer to the detumbling mode after the booting; the magnetic control function is initialized by the flight software to stable the satellite when angular rate is higher than a threshold. Then, it transmits the SOH data in Morse code format via TT&C subsystem module for ground station

tracking.

In the mission mode, the satellite follows the uplink telecommands and is scheduled to execute the flight software. It collects housekeeping telemetry and science data, then stores in OBDH storage device (SD Card) for a later downlink. The science data include EFP, MAG, TeNeP, TIP and IP measurements.

When the voltage is lower than the pre-setting threshold, the detector generates an interrupt signal to the onboard processor for safety mode transition. The flight software will turn off all the non-essential subsystems and disable the attitude control to save the power and recharge the batteries. As satellite executes the communication operation, TT&C subsystem standby to receive commands or transmit telemetry. In addition, the error message of satellite will be saved and if the number of errors is higher than a pre-set threshold, the satellite will save an error detect report (EDR) and reboot the system. The EDR will be sent with telemetry data in next contact.

Table2.17 Description of the operation modes

Spacecraft Mode	Description
Booting mode	Re-establishing communication between the spacecraft and mission control, downloading any diagnostic data and sequencing power back on to the various subsystems to resume the mission.
Detumbling mode / Nominal mode	Checking angular-rate and de-tumbling of the spacecraft as well as to recover it from any spin-ups after booted FSW or return from safe mode. In addition to the essential components that are ON all the time, the ADCS is also operational during this mode. Any other device could be turn ON by ground command.
Safe mode	This mode is intended to keep the satellite alive. All non-essential systems, such as scientific instruments, are shut down. The spacecraft awaits telecommands. Only the necessary components are ON all the time, such as the OBC, EPS and VHF receiver. Transmitter is turned ON occasionally.
Data Dump *(Communication mode)*	This mode is used when the satellite establish contact to the Ground Station. All systems are turn ON except Payload.
Mission Mode	This mode collects housekeeping telemetry and science data, storing them in storage device on OBDH. All the scientific payloads are powered on.

3. Anticipated results

The AICE mission investigates the electrical coupling processes between the ionosphere and atmosphere, even lithosphere. These processes including lightning-driven electron enhancement and disturbance caused by earthquakes are still not well known to scientists. However the understanding of these processes may be helpful in the applications of the disaster prevention, communication and space weather forecast. The AICE mission is expected to contribute significately in the following research and applications.

From the view of education, participating students in this mission can practically implemente what they learned in the courses of space and plasma sciences, as well as space engineering technology by developing and operating this student-oriented AICE mission. The AICE microsat is compact and highly modualized and can also act as a common platform for the mission in the future.

4. Originality and/or social effects

In the science, the AICE mission is proposed firstly to monitor the coupling process between ionosphere and atmosphere globally by an in-situ measurement on the plasma characteristics, electromagnetic fields. The observation may be able to provide scientific evidence to learn how lightning, thunderstorm and earthquake disturb ionosphere. The impact of this mission is not only essential to the precursor of the earthquake which greatly receive public attentions and is important to the development on the disaster prevention, but is helpful to understand the imapct of the thunderstorm to the ionosphere, and its probable contribution to the global electric circuit.

By developing the AICE mission, participating students gain hands-on experiences through the systematic analysis, manufacturing and testing on the satellite bus and the scientific payloads. The AICE mission also acts as an excellent platform for training space-related engineers and scientists. To satisfy the tough requirements in the space mission, the quality demands on the components, payload and bus will also promote associated local industries.

5. Concrete achievement methods, range and budget for manufacturing

This AICE microsatellite will be developed by the NCKU team, associated with several institutes including Physics, Plasma and Space Science, Earth Science, Aeronautics & Astronautics, Electrical Engineering department in NCKU. During the satellite development,

The existing equipments and facilities distributed among institutes are used for the fabrication, test, calibration and integration in this mission, including the space plasma chamber (2m in diameter and 3m in length), Class 100K clean room, 130 keV ion beam system, thermal cycling chamber, vibration test platform, network analyzer, spectrum analyzer,

signal generator, oscilloscope, NI-PXI for satellite hardware development, and Matlab, LabVIEW, and ANSYS software for satellite analysis and simulation. Some large facilities, for example thermal vacuum chamber, will be supported by National Space Organization, Taiwan.

The preliminary cost is listed in the following. The preliminary estimated budget is about 0.45 million US dollars for a single satellite development and manufacture.

Table2.18 Cost Breakdown

Components	Estimated cost (USD)
Structure	20,000
UHF band Transceiver and S-Band transmitter	40,000
Solar Cells	200,000
PDRU	20,000
ADCS sensors	30,000
ADCS flywheels	30,000
ADCS magnetic torques	25,000
C&DH	15,000
TeNeP	2,000
IP	15,000
EFP	20,000
MAG	3,000
TIP	20,000
Misc.	10,000
Total	**450,000**

6. Development, manufacture and launch schedule

The development of AICE is scheduled to complete within three years. The design review meetings are essentially held during the satellite development. After kick-off meeting, the mission objective, mission requirement is decided. In satellite part, orbit element specification definition, satellite mechanical/electrical requirement definition, design analysis and satellite bus/payloads architecture design is conducted already. Before preliminary design review (PDR), the mission analysis will be verified. The key components will be acquired and put into implement for purchase processing. Flight software coding will start at the same time with onboard hardware implement and installation. Before critical design review (CDR), the integration and test of the AICE hardware and software will be in process and expected to be completed certainly. After that, the complete satellite will be assembled and integrated by NCKU team. In addition, the environment test will be conducted after the integration and test

review (ITR). After all detail has been checked, a launch vehicle (LV) interface meeting should be held with the LV provider to discuss and define the interface between AICE and LV. After all, the AICE is ready to ship to launch site and integrate with launch vehicle. After AICE launched, one year mission life is predicted and can be extended to two years for the electrical coupling study.
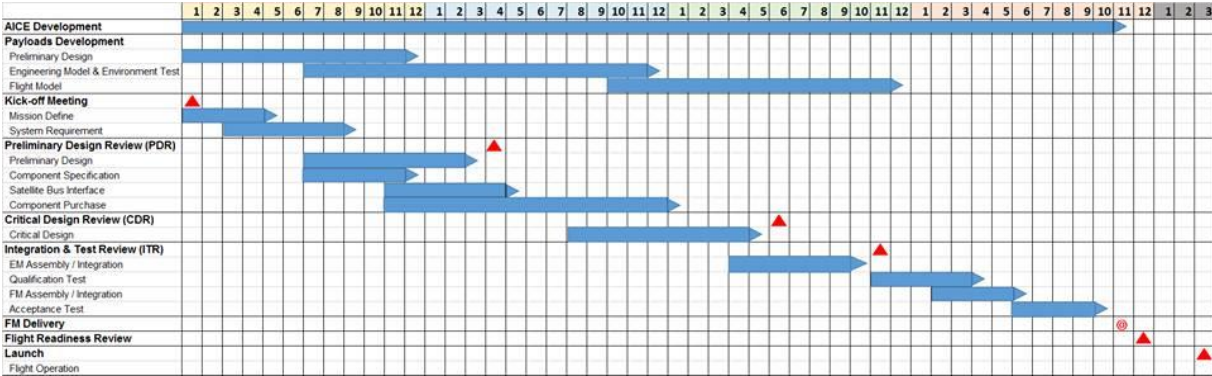

Figure6.1 Development schedule of AICE

7. Conclusion

The AICE mission is dedicated to the study of the coupling process between near earth region to ionosphere, which is possibly related to earthquake precursors and the plasma irregularities driven by thunderstorm. To achieve this objective, five scientific instruments are developed to have in-situ measurement for plasma characteristics, electric and magnetic fields at the altitude of 300-700km height. The NCKU team has done the preliminary analysis on the mission science, system design, orbit analysis, and the flexibility study of the scientific payloads. The technical readyness level (TRL, see Figure 7.1) shows that this mission is workable and the techincal challenge may be not too difficult. The participated students gain hands-on experience from the space qualified development and test. The AICE mission is also a platform for space engineering and space science education. Further, the AICE mission will be a pioneer of near earth electrical coupling process research.

Table7.1 The technical readyness level of AICE mission

Subsystems	TRL	Payloads	TRL
SMS	TRL 8-9	EFP	TRL 7-8
TCS	TRL 8-9	MAG	TRL 9
ADCS	TRL 8-9	TeNeP	TRL 7-8
EPS	TRL 8	IP	TRL 9
C&DH	TRL 8-9	TIP	TRL 9
TT&C	TRL 8-9		

8. Reference

[1] Davies, K., and D. M. Baker , Ionospheric effects observed around the time of the Alaskan earthquake of March 28, 1964, J. Geophys. Res., 70, 2251–2253, doi:10.1029/JZ070i009p02251,1965.

[2] Moore, G. W., Magnetic disturbances preceding the 1964 Alaska earthquake, Nature, 203(4944), 508–509, doi:10.1038/203508b0,1964.

[3] Liu, J. Y., et al., Seismo-ionospheric GPS total electron content anomalies observed before the 12 May 2008 Mw7.9 Wenchuan earthquake, J. Geophys. Res., 114, A04320, doi:10.1029/2008JA013698,2009.

[4] Kuo C. L. ,Huba J. D., Joyce G., and Lee L. C., Ionosphere plasma bubbles and density variations induced   by pre-earthquake rock currents and associated surface charges, J. Geophys. Res., VOL. 116, A10317, doi:10.1029/2011JA016628, 2011

[5] Le Huijun, Liu Libo, Jann-Yeng Liu, Biqiang Zhao, Yiding Chen, Weixing Wan,The ionospheric anomalies prior to the M9.0 Tohoku-Oki earthquake, Journal of Asian Earth Sciences 62   476–484, (2013).

[6] M. Gousheva, D. Danov, P. Hristov1, and M. Matova, Ionospheric quasi-static electric field anomalies during seismic activity in August–September 1981, Nat. Hazards Earth Syst. Sci., 9, 3–15, 2009

[7] U. S. Geological Survey website http://earthquake.usgs.gov/earthquakes

[8] Velinov, P.I.Y. and Tonev, P.T., Park C. G. and Dejnakarintra M.,Penetration of thundercloud electric fields into the ionosphere and magnetosphere: 1. Middle and subauroral latitudes, Volume 78, Issue 28, pages 6623–6633, 1 October DOI: 10.1029/JA078i028p06623,1973. Thundercloud electric field modeling for the ionosphere-Earth region: 1. Dependence on cloud charge distribution., J. Geophys. Res., Vol 78, Issue 28, 6623–6633, doi: 10.1029/94JD00286. issn: 0148-0227,1995.

[9]   Fukunishi, H., Y. Takahashi, M. Kubota, K. Sakanoi, U. S. Inan, and W. A. Lyons, Elves: Lightning-induced transient luminous events in the lower ionosphere, *Geophys. Res. Let.*, *23*, 2157-2160, 1996.

[10] Hu, W., S. A. Cummer, W. A. Lyons, and T. E. Nelson, Lightning charge moment changes for the initiation of sprites, Geophysical Research Letters, v. 29, no. 8, 1279, doi:10.1029/2001GL014593, 2002.

[11] Pasko, V. P., U. S. Inan, T. F. Bell, and Y. N. Taranenko, Sprites produced by quasi-electrostatic heating and ionization in the lower ionosphere, *J. Geophys. Res.*, *102*(A3), 4529-4561, 1997.

[12] Pasko, V. P., Electric jets, *Nature*, 423, pp. 927-929, 2003.

[13] Krehbiel, P. R., et al., Upward electrical discharges from thunderstorms, *Nat. Geosci.*, 1, 233–237, doi:10.1038/ngeo162, 2008.

[14] Asada, S., Abe, N., Andoh, K., Fleeter, R., Launching Small Satellites on the H-IIA Rocket

[15] Paschmann, G., McIlwain, C. E., Quinn, J. M., Torbert, R. B., and Whipple, E. C.: in: The electron drift technique for measuring electric and magnetic fields, (Eds) Pfaff, R. F., Borovsky, J. E. and Young, D. T., Measurement Techniques in Space Plasmas: Fields, 29–38, Geophysical Monograph 103, AGU, Washington, D. C., 1998.

[16] Mozer, F. S.; Cattell, C. A.; Temerin, M.; Torbert, R. B.; von Glinski, S.; Woldorff, M.; Wygant, J., The dc and ac electric field, plasma density, plasma temperature, and field-aligned current experiments on the S3-3 satellite, *J. Geophys. Res.*, vol. 84, 5875-5884., DOI: 10.1029/JA084iA10p05875, 1979.

[17] Maynard N. C. , Burke W. J. , Weimer D. R., Mozer F. S., Scudder J. D.,   Russell C. T., Peterson W. K., Lepping R. P., Polar observations of convection with northward interplanetary magnetic field at dayside high latitudes, Vol 103, A1, 29–45,Volume 103, Issue A1, pages 29–45, 1 January 1998, 1998

[18] Hong, Zuu-Chang, Lin, Chien-Ming, Chang, Bo-Jyun, The design of a low-cost gravity-gradient boom for microsatellite, Journal of technology, Vol. 22, No. 4, pages 315-323, 2007

[19] Bradford, Keith R., Miniature Wire Boom System for Cubsat Application, All Graduate Plan B and other Reports. Paper 259,pages 25-64, May 2013,2013